Growth of Pt/Cu(100): an atomistic modeling comparison with the Pd/Cu(100) surface alloy

Gustavo Demarco[a], Jorge E. Garcés[a,b] and Guillermo Bozzolo[b,c*]

[a] *Centro Atómico Bariloche, 8400 Bariloche, Argentina*
[b] *Ohio Aerospace Institute, 22800 Cedar Point Rd., Cleveland, OH 44142, USA*
[c] *NASA Glenn Research Center, Cleveland, OH 44135, USA*

Abstract

The BFS method for alloys is applied to the study of Pt deposition on Cu(100). The formation of a Cu-Pt surface alloy is discussed within the framework of previous results for Pd/Cu(100). In spite of the fact that both Pd and Pt share the same basic behavior when deposited on Cu, it is seen that subtle differences become responsible for the differences in growth observed at higher coverages. In agreement with experiment, all the main features of Pt/Cu(100) and Pd/Cu(100) are obtained by means of a simple modeling scheme, and explained in terms of a few basic ingredients that emerge from the BFS analysis.

Keywords: Adatoms; Computer Simulations; Copper; Platinum; Palladium; Semi-empirical methods and model calculations; Surface Alloys; Surface structure.

1. Introduction

The Cu-Pt system has been the subject of numerous studies including direct or indirect analysis of the formation of a Cu-Pt surface alloy for different substrate orientations. The studies range from the deposition of Cu on a Pt substrate [1-6] to the study of the surface composition of ordered alloys [7] or the deposition of Pt on a Cu substrate[8-14].

Deposition of Cu on Pt(111) was studied by Tsay et al. [1], who used Auger electron spectroscopy (AES) to study the formation of $Cu_{50}Pt_{50}(111)$ bilayer surface alloys. For the same system, Holst et al. [2] discussed the growth of ultrathin Cu films using scanning tunneling

microscopy (STM). Cu deposition on Pt(100) was also studied using STM and low-energy electron diffraction (LEED), indicating the growth of epitaxial Cu films [3-6].

Pt deposition on a Cu substrate has also been thoroughly investigated [8-14]. Cu-Pt intermixing was also observed by Shen et al. [8] using low energy ion spectroscopy (LEIS) for the study of Pt/Cu(111) thin film growth. The epitaxial growth of Pt leads to a metastable Cu_3Pt surface alloy at 573 K. In related studies, the surface composition of a $Cu_3Pt(100)$ alloy was determined using LEIS and LEED [7], concluding that a c(2x2) Cu-Pt second layer alloy forms below a (1x1) Cu termination. The basic structure of the c(2x2) is shown in Fig. 1.a. A LEIS analysis by the same authors [9] determined the surface composition of a $Cu_3Pt(110)$ alloy showing a mixed surface layer followed by a pure Cu underlayer. Dispersed Pt atoms in a Cu matrix were found by Schroeder et al. [11] in a study of the adsorption properties of Pt/Cu(111). Pt bulk dissolution was observed in the thermal energy atom scattering analysis of Pt/Cu(110) by Hugenschmidt et al. [14]. Finally, attention has been paid to the deposition of Pt on Cu(100) [10,13]. The work of Belkhou et al. [10] indicates that Pt deposition leads to a Cu-Pt surface alloy, with a Pt surface concentration of 50%, consistent with the observed c(2x2) LEED pattern. For higher Pt coverage (> 2 ML), the surface alloy disappears and pure and disordered Pt films start to grow. These results are consistent with the LEED and AES analysis of Reilly et al. [13] indicating submonolayer Pt growth leading to the formation of a poorly ordered surface alloy, with Cu on the surface layer followed by a c(2x2) structure in the second layer.

It is interesting to compare Pt/Cu(100) surface alloys to the Pd/Cu(100) [15] case, as both evolve into a c(2x2) structure but with marked differences during the growth process. A strong tendency towards surface alloy formation is expected for the Pt/Cu(100) system since the bulk mixing enthalpy is exothermic. The same is true for the Cu-Pd system, but the fact that Pt has a significantly higher surface energy than Pd suggests that differences in the geometry of the surface alloy could be expected. It is well known that Pd deposition on Cu(100) results in high-quality c(2x2) LEED patterns [15] at submonolayer coverages upon deposition at room temperature. Some Pd dissolution in subsurface layers is also observed. In contrast, the Pt/Cu(100) system is not as well characterized. Pt adsorption leads to a somewhat random pattern of Pt substitutions in the Cu substrate at low coverages. However, the formation of a well ordered surface requires Pt coverages slightly in excess of 0.5 ML and thermal activation to 530K, while annealing above this temperature leads to slow dissolution of Pt in the bulk [13]. It is therefore interesting to analyze, in

some detail, the differences and similarities in these otherwise comparable systems, in order to gain much needed detail and therefore understanding in the surface alloy formation processes of both systems.

The BFS method for alloys [16], a quantum approximate method for atomistic modeling, has been applied to the Cu-Pd system, successfully reproducing the observed behavior in Pd/Cu(100), Pd/Cu(110) and Cu/Pd(100) [17]. In this work, we present results of a modeling effort at the atomic level, also based on the BFS method for alloys, meant to elucidate the main characteristics of the early growth stages of Pt on Cu(100), comparing the results with a similar process for Pd on Cu(100).

2. The BFS method

The BFS method [16] is based on the concept that the energy of formation of a given atomic configuration is the superposition of the individual atomic contributions $\Delta H = \Sigma\, \varepsilon_i$. Each contribution by atom i, ε_i, is the sum of two terms: a strain energy, ε_i^S, computed in the actual lattice as if every neighbor of the atom i was of the same atomic species i, and a chemical energy, ε_i^C, computed as if every neighbor of the atom i was in an equilibrium lattice site of a crystal of species i, but retaining its actual chemical identity. The computation of ε_i^S, using Equivalent Crystal Theory (ECT) [18], involves three pure element properties for atoms of species i: cohesive energy, lattice parameter and bulk modulus. The chemical energy, ε_i^C, includes two BFS perturbative parameters (Δ_{CuPt} and Δ_{PtCu}) [16]. A reference chemical energy, ε_i^{Co}, is also included to insure a complete decoupling of structural and chemical features. In this work, all the necessary parameters were determined by fitting the BFS predictions to the experimental heat of solution in the dilute limit [19]. Finally, the strain and chemical energies are linked with a coupling function g_i, which ensures the correct volume dependence of the BFS chemical energy contribution. Therefore, the contribution of atom i to the energy of formation of the system is given by

$$\varepsilon_i = \varepsilon_i^S + g_i(\varepsilon_i^C - \varepsilon_i^{C_0}) \qquad (1)$$

Table I lists the necessary parameters for applying the BFS method to the Cu-Pd and Cu-Pt systems. We refer the reader to Refs. 16 and 18 for a detailed discussion of the BFS method, its definitions, operational equations and their implementation.

3. Results

From the modeling standpoint, more can be learned about the subtle mechanisms of surface alloy formation through the deposition of Pt on Cu(100) if it is analyzed in comparison with the previous results found for Pd/Cu(100). This is due to the fact that in both cases, the basic step in the beginning of the alloy formation process is the insertion of a Pt (or Pd) atom in a surface site, with the ejected Cu atom in a nearest-neighbor (NN) site in the overlayer. However, in spite of this similarity, the atomic interactions are different in each case, thus leading to different surface alloy patterns with increasing coverage. In what follows, an atom X (X = Pd, Pt, Cu) occupying a site in layer Y (Y = overlayer (O), surface (S), first (1b) and second (2b) plane below the surface), will be denoted with X(Y). A pair of atoms can be then denoted with $X_1(Y_1)X_2(Y_2)_d$, where d denotes the distance between atoms X_1 and X_2. The distance d can be 1, 2 or f, depending on whether X_1 and X_2 are NN, next-nearest-neighbors (NNN) or farther apart, respectively.

Fig. 2 shows atomic configurations corresponding to one deposited Pd or Pt atom. These include the adatom in the overlayer (X(O)), in the surface layer with the ejected Cu atom in a NN site in the overlayer ($X(S)Cu(O)_1$) or away from the inserted atom ($X(S)Cu(O)_f$)). Two states showing the X atom in the first and second layer below the surface are also shown (X(1b)Cu(O) and X(2b)Cu(O), respectively. The energy level spectra for these states are nearly identical, showing preference for substitution of surface Cu atoms. The lowest energy state corresponds to the structure $X(S)Cu(O)_1$. It is immediately followed by $X(S)Cu(O)_f$, and by states showing interdiffusion of X to the first (1b) and second (2b) plane below the surface (S), as shown in Fig. 3. There is also a striking similarity between the separation between the energy levels if those energy differences are measured relative to the difference in energy between X(O) and the ground state ($X(S)Cu(O)_1$).

However, a similar analysis for two adatoms allows us to identify substantial differences between the growth patterns of Pd/ and Pt/Cu(100). It is already at this very low coverage that the seed of a c(2x2) pattern is observed for Pd/Cu(100) and a p(2x2) for Pt/Cu(100). To fully understand the observed behavior, it is important to scan the whole spectrum, besides just focusing on the lowest energy state. Fig. 4 shows some of the most important configurations, and Fig. 5 shows the corresponding energy level spectra. The highest energy state, in both cases, corresponds to a

dimer in the overlayer, $X(O)X(O)_2$ (X = Pd, Pt), indicating that the formation of a surface alloy is favored over epitaxial growth. The ground state 'band' for Pt/Cu(100) (i.e., the cluster of energy levels at the bottom of the spectrum) indicates a clear preference for a p(2x2) arrangement, followed by a number of states characterized by the varying proximity between the substituted Pt(S) atoms. It is interesting to note that the state closest to the lowest energy state allows the insertion of nearest-neighbor Pt(S) dimers, with a peculiar location for the displaced Cu(O) atoms. Due to the high energy of a similar arrangement where the Cu(100) atoms fully 'link' the Pt(S) atoms (Fig. 4.c), it is clear that the location of the Cu(O) atoms is responsible for the low energy of the state shown in Fig. 4.h. After a small energy gap, a state displaying c(2x2) ordering appears (Fig. 4.g). In contrast with this energy level distribution, the Pd/Cu(100) spectrum displays a reversal between the p(2x2) and c(2x2) states, favoring the formation of a c(2x2) structure, with a much smaller energy gap between these two types of patterns with respect to the Pt/Cu(100) case. This can be explained by the fact that, at this level of coverage, a p(2x2) structure can be thought of as an 'incomplete' c(2x2) structure, as it only takes one additional substitution to complete a c(2x2) pattern from a p(2x2) one. In other words, a p(2x2) structure sets a lower bound for proximity between the substituted atoms: if the p(2x2) structure is the lowest one in energy (as is the case for Pt), it takes a large energy cost to build a c(2x2) structure, as it implies locating atoms at closer distances than what a p(2x2) allows. Conversely, a smaller energy cost is necessary to build a p(2x2) from a c(2x2) structure (as is the case for Pd).

Fig. 6 shows three possible coupling schemes between X(S) and Cu(O) (X = Pd, Pt) atoms and their respective energy differences with the lowest energy configuration (among the set of configurations shown). In the Pd/Cu(100) case, the Pd atoms in the surface sites exhibit c(2x2) growth, where two Pd atoms are located in next-nearest-neighbor (NNN) sites sharing one of the ejected Cu atoms (Fig. 6.a), thus maximizing coordination for the whole set of atoms. In the case of Pt/Cu(100) the opposite is true. Pt atoms 'repel' each other, only linking through the Cu(O) atoms (Figs. 6.b and 6.c), with the lowest energy state being the one where Pt atoms are not interacting at all.

As the coverage increases, the analysis is greatly simplified by noting that Cu(O) atoms will naturally tend to form compact islands, as seen already in the N = 2 case. As a result, it is only necessary to examine configurations where the Pt(S) (or Pd) atoms are linked, in different ways, to the compact Cu(O) island. The 'repulsion' between Pt atoms, hinted by the maximum separa-

tion in the case N = 2 (see Fig. 6.c), would lead to configurations with low symmetry and higher energy. For example, Fig. 7 shows a representative set of configurations for N = 3, covering the whole energy spectrum both for Pd and Pt. In spite of the similarities between the Pd and Pt spectra for N=1, it is clear now that at this level of coverage, the competition between the attraction of Pt(S) and Cu(O) atoms and the 'repulsion' between Pt(S) atoms, is the driving force for the emergence of the observed ordering pattern. As expected, those configurations that maximize the distance between Pt(S) atoms are greatly favored. Not surprisingly, the lowest energy configuration corresponds to a p(2x2) pattern (Fig. 7.a). The differences between Pd and Pt now become apparent, as the lack of 'repulsion' between Pd atoms favors a c(2x2) arrangement (Fig. 7.d), as hinted already in the case N=2 (Fig. 6.a).

The addition of another Pt (or Pd) atom does not introduce new features in the growth process at this level of coverage. The lowest energy state for N=4 continues to be a p(2x2) structure for Pt, and a c(2x2) structure for Pd. Fig. 8 shows these states and the energy gap between them, both for Pd and Pt. As the coverage increases, and as long as the island of ejected Cu(O) atoms is required to remain 'attached' to the substitutional Pt(S) (or Pd(S)) atoms, it is seen that it is not possible to continue the growth of the surface alloy following a p(2x2) pattern covered with a Cu island without allowing for other possibilities. It becomes harder to continue this pattern with the available Cu(O) atoms.

Similar configurational analyses for N > 4 indicate that the lowest energy state is a p(2x2) patch with additional Pt(S) located at distances smaller than those necessary for the continuation of a p(2x2) pattern. Not surprisingly, those 'bare' Pt(S) atoms locate themselves in surface sites that follow, instead, a c(2x2) pattern, as can be seen in Fig. 9, where the lowest energy states for N=5, N=6, and N=8 are shown. This could be interpreted as if the Cu(O) island has a stabilizing effect on the formation of the p(2x2) structure for Pt but not for Pd. Before discussing the feature found for N>4, shown in Fig. 9, it is useful to investigate further the N=4 case, by comparing configurations that differ in the location of the Cu(O) island. So far, all the N=4 states were based on the nucleation of a specific pattern in direct relationship to the island attached to it. It remains to be seen if a different alloying behavior arises in the absence of such islands. This is clearly seen in Fig. 10: the lowest energy state for Pd is always the c(2x2) structure with an attached Cu(O) island (Fig. 10.b), followed by the p(2x2)+island and then, much higher in energy, the same structures but with the island somewhere else. The situation is different for Pt: the lowest energy state

corresponds to the p(2x2) + island configuration, followed by the c(2x2) with no island, indicating that the p(2x2) structure is stabilized by the proximity of the island, and that the c(2x2) pattern is preferred in its absence.

With this new information in mind, we return to the analysis of Fig. 9, considering the role of the island in the structure of the ground state for N>4. For N=5, the lowest energy state, both for Pd and Pt, can be described as a mixture of a c(2x2) and a p(2x2) patch, as shown in Fig. 9.a. In the case of Pd, this is a natural continuation of the pattern observed for smaller values of N. For Pt, the lack of enough Cu(O) atoms to provide the optimum conditions for developing the p(2x2) pattern, makes the additional Pt(S) atom take a 'c(2x2)' site. This is observed again in the case N=6 (Figs. 9.b-d), where the c(2x2) structure is the lowest energy state for Pd (Fig. 9.b) but a combination of 'covered' p(2x2) and an 'uncovered' c(2x2) is observed for Pt. It is clear that a full p(2x2) pattern is not favored by either element (Fig. 9.d). The N=8 case shows an additional feature in the case of Pd: the two lowest energy states correspond to compact c(2x2) patches (Fig. 9.e-f). However, more than one arrangement is possible, and the less intuitive one has lower energy (Fig. 9.e), suggesting that the atoms will locate themselves in 'c' sites, but following specific rules that seem to optimize the coordination and number of favorable bonds. That is not the case, once again, for Pt, where the stabilizing effect of the Cu(O) island is clearly demonstrated by the superposition of a p(2x2) patch (center of Fig. 9.h) and a c(2x2) patch (upper right and lower left ends of the surface alloy patch). As the coverage increases, and as long as Cu(O) atoms are only available from Pt(O) -> Pt(S)Cu(O) substitutions, the rate of growth of a compact Cu island is such that the formation of a c(2x2) is favored, thus leading, as observed experimentally [10], to a c(2x2) structure for 0.5 ML Pt coverage. Therefore, the Pt deposition on Cu(100) can be summarized by the sequence of a p(1x1), p(2x2), a 'mixed' p(2x2) and c(2x2), and c(2x2) patterns, with increasing Pt coverage. In addition, the calculations also show that this sequence is highly dependent on the interaction between the surface alloy and the stabilizing role of the islands formed by the ejected Cu atoms.

It is also interesting to note that Pt interdiffusion in Cu is expected, like in the Pd/Cu(100) case. In spite of the higher strain induced by larger Pt atoms inside the Cu substrate, the alloying effect of the strong Pt-Cu bonds results in Pt interdiffusion, which would lead to the formation of a mixed phase in the near-surface layers. This is in agreement with the observations of the surface structure of Cu-Pt alloys as well as in the deposition of Pt/Cu or Cu/Pt [7,8,9,15]. Fig. 11 high-

lights this result, by showing the evolution of a state where the atom occupies a site in the first (1b) or second (2b) layer below the surface. In both cases, the energy gap between the corresponding ground state for each coverage, and the energy of the configuration where the atom resides in the 1b or 2b layer, becomes smaller, indicating an increasing likelihood - more noticeable for Pt than for Pd - that the atom will penetrate the surface layer. Once inside, however, it is necessary to include relaxations in the calculations in order to account for every possible structural feature [14].

Discussion

It is interesting to further analyze the differences and similarities between Pd/Cu(100) and Pt/Cu(100) in terms of the behavior of individual atoms, and therefore attempt to understand each and every feature described in the previous section.

The first point is the similarity between the Pd and Pt one-atom spectra, shown in Fig. 3. They are nearly, but not completely, identical. If they were, then there should be no difference in the behavior at higher coverages, as discussed in the previous section. It is likely then that the N = 1 spectra carry the information that will later translate into the different behaviors seen already for N = 2. The only qualitative difference between the spectra is the location of the $X(S)Cu(O)_f$ state relative to the ground state, $X(S)Cu(O)_1$. The fact that the former is a lower energy state for Pt than for Pd, means that Pt does not need the proximity of Cu(O) as much as Pd does in order to stabilize the substitution with surface atoms. The difference in the magnitude of the gap between the two lowest energy levels, $X(S)Cu(O)_1$ and $X(S)Cu(O)_f$ (X = Pd, Pt), can be identified as the source of the ensuing behavior observed for higher coverage. To gain a better understanding of the source of such difference, we performed an atom-by-atom calculation of the corresponding configurations, as illustrated in Fig. 12 and Table 2. The most noticeable feature in any of the entries in Table 2 is the fact that the chemical energy of Cu or X atoms is always negative, as long as they have each other as nearest or next-nearest neighbors, indicating, within the context of BFS, that both atoms would favor the formation of a Cu-X alloy. However, while the behavior of the affected Cu atoms is largely the same both for Pd or Pt additions, the 'strength' of Pd(S) or Pt(S) as nucleation points is the net result of the competition between BFS strain and chemical effects for those atoms. To illustrate this point, we first study the $Pt(S)Cu(O)_f$ case (Fig. 12.a), where the

Pt (S) atom is surrounded by just eight nearest-neighbors. In spite of the fact that the lattice spacing for Cu (3.615 Å) is smaller than the equilibrium lattice parameter of Pt (3.92 Å), there is still a substantial strain energy contribution (0.561 eV/atom) due to the reduced coordination. This translates into a rather small value of the coupling function g (0.59535) which reduces the effect of the favorable chemical Cu-Pt bonds. The net result is a total contribution of 0.20646 eV/atom to the total energy of formation. The same atom in $Pt(S)Cu(O)_1$ (Fig. 12.b), by having an extra Cu atom (Cu(O)) as a NN, increases its coordination and therefore reduces the strain energy to just 0.18715 eV/atom, thus increasing the value of the coupling function g (0.75796), yielding a total favorable contribution of –0.22171 eV/atom to the total energy of formation. A similar analysis for Pd(S) in either configuration shows that the same factors come into play to make $X(S)Cu(O)_1$, for both elements, the lowest energy state. However, even in $Pd(S)Cu(O)_1$, the contribution of the Pd atom to the total energy is never negative. It is interesting to note that two ingredients in the calculation of the strain energy of Pt cancel each other. On the one hand, the lack of coordination is a source of increased strain, both for Pt and Pd. On the other hand, the fact the lattice mismatch between Pt and Cu is larger than that of Pd and Cu, clearly favors Pt, as it compensates its reduced coordination with increased proximity of the neighboring atoms. As a result, while the Pt(S) atom is in a nearly ideal strain situation (the net strain energy is just 0.18175 eV/atom), a Pd atom in the same site has a strain energy of 0.34690 eV/atom. In addition, the reduced strain energy of Pt (relative to Pd), increases the value of the coupling function g, thus magnifying the effect of the favorable bonds (i.e., large negative chemical energy), resulting in a more favorable contribution to the total energy of formation of the cell. Therefore, a combination of the increase of Pd strain due to reduced coordination and weaker chemical bonds between Pd and Cu, makes Pd(S) a stronger nucleation site than Pt(S), which can afford losing its Cu(O) NN more than Pd(S) can.

It is interesting to analyze, in a similar fashion, the atom-by-atom contributions in the c(2x2) and p(2x2) patches shown in Fig. 8. Table 3 lists the total energy of formation of the computational cell in each case, as well as the strain and chemical components. The total energy results indicate a slight advantage for Pt/p(2x2) over Pt/c(2x2), while the opposite is true for Pd. The mechanisms, however, are slightly different in each case. For Pt, there are both overall strain and chemical gains in the p(2x2) patch, whereas for Pd a small increase in strain is offset by a lower chemical energy, giving a slight edge to the c(2x2) patch. It is therefore clear that a delicate balance between the strain and chemical energies of each affected atom must be achieved in order to

stabilize either structure. Table 4 lists the contributions per layer to the total energy. In both cases, the layer 1b favors the insertion of Pt or Pd in the surface layer, more so for a c(2x2) patch than for a p(2x2) one. Moreover, the four atom cluster of Cu(O) atoms is also favored by the formation of a Pt or Pd c(2x2) patch underneath. It is in the surface layer where the energy gains are realized and ultimately favor a p(2x2) for Pt and a c(2x2) patch for Pd. More insight can be gained from examining the individual contributions of each non-equivalent atom in each case, as listed in Table 5. The compact nature of the c(2x2) patch favors the Pt(S) atoms, which approach full coordination, minimizing the strain contribution (0.00343 eV/atom), and as a result, optimizing the coupling function (g=0.96595) and thus the favorable chemical energy contribution. The total energy contribution of Pt(S)/c(2x2) is –0.35238 eV/atom, a sharp improvement on the –0.22171 eV/atom contribution in p(2x2). The gain in energy that stabilizes Pt/p(2x2) vs. Pt/c(2x2) is then provided by the remaining Cu(S) and Cu(1b) atoms which, due to the spread of Pt(S) on the surface layer, maximize the number of Pt-Cu bonds.

A similar analysis for Pd results in the opposite behavior due mostly to the energy gains realized by the Cu(O) island and the Cu(1b) layer, as shown in Table 4. On a layer-by-layer basis, the contributions in the Pd case follow the same trend, as shown in Table 4, only that the balance of strain and chemical energy now favors the Pd(S)/c(2x2) over the p(2x2) patch. The low coordination of the Pd(S) atoms in the p(2x2) patch, results in high strain (0.3469 eV/atom) and a net positive contribution to the total energy. The Pd addition thus favors a c(2x2) arrangement, optimizing both the coordination (nearly ideal in a c(2x2) patch) and, consequently, the chemical energy contribution of each Pd(S) atom (-0.31223 eV/atom). Fig. 13 shows a diagram of each patch and the individual contributions from each affected atom are listed in Table 5.

Moreover, the availability of additional Cu(O) atoms emphasizes this trend for Pd and Pt: a more noticeable energy gain is realized for Pd when a second Cu(O) atom bonds to the ground state in Fig. 3 (0.61 eV/atom) than for Pt (0.44 eV/atom), indicating that a $Pd(S)Cu(O)_1Cu(O)_{11}$ cluster will be preferred over a single $Pd(S)Cu(O)_1$ one. This helps explain the competition between the configurations shown in Figs. 9.e and 9.f. As mentioned in the previous section, the compact c(2x2) patch shown in Fig. 9.f is less favorable energetically than the one shown in Fig. 9.e, as the latter maximizes the number of Pd(S) atoms attached to the two Cu(O) atoms, even at the expense of leaving one 'bare' Pd(S) atom outside the c(2x2) patch (top left corner of Fig. 9.e). As a consequence, Pd will seek greater coordination with ejected Cu(O) atoms, thus leading to a

c(2x2) structure where each Pd(S) atom shares two Cu(O) atoms, as opposed to Pt in the p(2x2) structure, where only one such neighbor is present. Therefore, it can be concluded that all the ingredients necessary to explain the growth pattern, both for Pd and Pt, are already present in the N = 1 spectrum: the asymmetry of the $X(S)Cu(O)_f$ state for Pd and Pt, and a similar feature when a second Cu(O) atom intervenes. As a result, Pd needs a Cu(O) nearby, much more than Pt does (further substitutions will favor maximizing such proximity, therefore leading to a c(2x2) structure where such coalescence of Pd(S) and Cu(O) atoms is maximized). Also, it explains the stabilizing nature of the Cu(O) island (for Pt) and, for each coverage, the structure of the ground state.

Conclusions

The BFS method for alloys was applied to the analysis of the early stages of Pt growth on a Cu substrate. The results are compared, for each coverage, with a similar analysis of the Pd/Cu(100) surface alloy formation process showing that, in spite of the similarities at very low coverage, some basic differences account for the different growth patterns observed at higher coverages. The basic features that determine the growth pattern for each system are obtained by means of a BFS energy analysis of fundamental configurations and their corresponding energy level spectrum, with varying coverage. In doing so, it is shown that, at least in these cases, a full explanation of the growth process can be obtained from basic notions that characterize the interaction between the intervening atoms.

Acknowledgments

Fruitful discussions with N. Bozzolo are gratefully acknowledged. This work was supported by the International Computational Materials Science Consortium (OAI/NASA) and the HOTPC project at NASA Glenn Research Center.

References

[1] J. S. Tsay, T. Mange and K. Wandelt, Thin Solid Films 397 (2001) 152.

[2] B. Holst, M. Nohlen, K. Wandelt and W. Allison, Surf. Sci. 377-379 (1997) 891.

[3] N. M. Markovic, B. N. Grgur, C. A. Lucas, P. N. Ross, Electrochimica Acta 44 (1998) 1009.

[4] B. Willerding, K. Oster, J. Radnik, J. Braun and K. Wandelt, J. Electron Spectroscopy and Related Phenomena 93 (1998) 215.

[5] A. M. Bittner, J. Wintterlin, G. Ertl, Surf. Sci. 376 (1997) 267.

[6] J. Radnik, B. D. Wagner, K. Oster, K. Wandelt, Surf. Sci. 357-358 (1996) 943.

[7] Y. G. Shen, D. J. O'Connor and K. Wandelt, Surf. Sci. 406 (1998) 23.

[8] Y. G. Shen, D. J. O'Connor, K. Wandelt, R. J. MacDonald, Surf. Sci. 357-358 (1996) 921.

[9] Y. G. Shen, D. J. O'Connor and K. Wandelt, Surf. Sci. 410 (1998) 1.

[10] R. Belkhou, J. Thiele and C. Guillot, Surf. Sci. 377-379 (1997) 948.

[11] U. Schroeder, R. Linke, J.-H. Boo, K. Wandelt., Surf. Sci. 352-354 (1996) 211.

[12] N. T. Barret, R. Belkhou J. Thiele, C. Guillot, Surf. Sci. 331-333 (1995) 776.

[13] J. P. Reilly, D. O'Connell and C. J. Barnes, J. Phys.: Condens. Matter 11 (1999) 8417.

[14] M. B. Hugenschmidt and C. de Beauvois, Surf. Sci. 307-309 (1994) 455.

[15] Y. G. Shen, J. Yao, D. J. O'Connor, B. V. King and R. J. MacDonald, Solid State Comm. 100 (1996) 21.

[16] G. Bozzolo, J. Ferrante, R. D. Noebe, B. Good, F. S. Honecy, P. Abel, Comp. Mat. Sci. 15 (1999) 169.

[17] J. E. Garces, G. Bozzolo, H. Mosca and P. Abel, Surf. Sci. 482-485 (2001) 776.

[18] J. R. Smith, T. Perry, A. Banerjea, J. Ferrante, G. Bozzolo, Phys. Rev. B 44 (1991) 6444.

[19] G. Bozzolo and J. Ferrante, Phys. Rev. B 46 (1992) 8600.

TABLE CAPTIONS

Table 1: Experimental results for the lattice parameter (in Å), cohesive energy (in eV/atom), and bulk modulus (in GPa) for the fcc phases of Cu, Pd and Pt, and the resulting ECT [18] parameters p, α, l and λ [16,19] and BFS parameters Δ (in $Å^{-1}$).

Table 2: BFS strain and chemical contributions to the total energy of formation (in eV/atom) of the different non-equivalent atoms in the a) $X(S)Cu(O)_1$ and b) $X(S)Cu(O)_f$ configurations (Figs. 2.b-c). e^S, g, and e^C denote the strain coupling function and chemical energy, respectively. e_T denotes the total contribution (see Eq. 1). Each atom is labeled according to the location indicated in Fig. 12. The multiplicity m denotes the number of equivalent atoms and the label in brackets indicates the location of the atom in Fig. 12.

Table 3: Total strain, chemical energy, and total energy of formation (in eV/atom) of the computational cells shown in Fig. 8.

Table 4: Strain, chemical and total energy contributions per layer (in eV/atom) of the computational cells shown in Fig. 8.

Table 5: BFS strain and chemical contributions to the total energy of formation (eV/atom) of the different non-equivalent atoms in the a) X/p(2x2) and b) X/c(2x2) configurations (see text) (Figs. 8.a-b). e^S, g, and e^C denote the strain coupling function and chemical energy, respectively. e_T denotes the total contribution (see Eq. 1). Each atom is labeled according to the location indicated in Fig. 13. The multiplicity m denotes the number of equivalent atoms and the label in brackets indicates the location of the atom in Fig. 13.

FIGURE CAPTIONS

Fig. 1: Top view of a) a c(2x2) and b) p(2x2) structure, corresponding to 0.5 ML and 0.25 ML coverage, respectively. Substrate atoms are indicated with open circles.

Fig. 2: Side view of selected configurations for one adatom X (X = Pd or Pt) on a Cu(100) surface. X atoms (X = Pd, Pt) are denoted with large and small black disks, respectively. Displaced Cu(O) atoms are denoted with large disks and surface Cu(S) atoms are denoted with small circles. (a) an X atom in the overlayer (X(O)), the X atom in a surface site with the displaced Cu atom in a (b) distant overlayer site ($X(S)Cu(O)_f$)), or (c) in a nearest-neighbor site in the overlayer ($X(S)Cu(O)_1$), and an X atom in the (d) first (X(1b)Cu(O)) or (e) second (X(2b)Cu(O)) layer below the surface.

Fig. 3: Energy level spectra (in eV/atom)for a single Pd (left column) or Pt (right column) atom on a Cu(100) surface. The levels are located according to their energy relative to the difference in energy between the lowest ($X(S)Cu(O)_1$) and highest (X(O)) energy states (0.6393 eV/atom for Pd and 1.3451 eV/atom for Pt).

Fig. 4: Top view of selected configurations for two adatoms (Pd or Pt) on a Cu(100) surface. X(O) and X(S) atoms (X = Pd, Pt) are denoted with large and small black disks, respectively. Displaced Cu(O) atoms are denoted with large grey disks and surface Cu(S) atoms are denoted with small circles.

Fig. 5: Energy level spectra (in eV/atom) for two Pd (left column) or Pt (right column) atoms on a Cu(100) surface. The levels are located according to their energy relative to the difference in energy between the lowest and highest energy states. While the lowest energy state is different for Pd or Pt, in both cases the highest energy state corresponds to two adatoms located at next-nearest-neighbor distance ($X(O)X(O)_2$) (0.9610 eV/atom for Pd and 1.6579 eV/atom for Pt).

Fig. 6: Top view of a Cu(100) surface displaying different coupling schemes between two $X(S)Cu(O)_1$ 'defects' (X = Pd, Pt). In each case, the energies listed (in eV/atom) are referenced to

the lowest energy configuration. Cu(S), Cu(O) and X(S) atoms are denoted with open circles, large grey disks and black disks, respectively. The top line shows energy differences for Pd and the bottom for Pt.

Fig. 7: Top view of a Cu(100) surface showing different arrangements of three Pt atoms inserted in surface sites. In each case, the energies listed (in eV/atom) are referenced to the lowest energy configuration. The top line shows energy differences for Pd and the bottom for Pt. Cu(S), Cu(O) and X(S) atoms are denoted with small circles, large grey disks and black disks, respectively.

Fig. 8: Top view of a Cu(100) surface showing different arrangements of four Pt atoms (black disks) inserted in surface sites, forming (a) a p(2x2) and (b) a c(2x2) pattern. The configuration with the lowest energy of formation corresponds to a p(2x2) pattern for Pt/Cu, where the Cu(O) island (large grey disks) is attached to the p(2x2) patch. The top number indicates the difference in energy (in eV/atom) for Pd and the bottom line for Pt, in each case referenced to the lowest energy state. Cu(S) atoms are denoted with small circles.

Fig. 9: Top view of Pd or Pt atoms (black disks) inserted in Cu(100) surface sites for N = 5, 6, 8. Cu(S) and Cu(O) atoms are denoted with small circles and large grey disks, respectively. In each case, the difference in energy (in eV/atom) between a given configuration and the lowest energy configuration for that coverage is given both for Pd (top line) and Pt (bottom line).

Fig. 10: Top view of four Pt (or Pd) atoms (black disks) inserted in Cu(100) surface sites. The configuration with the lowest energy of formation (for Pt) corresponds to a p(2x2) pattern, where the Cu(O) island (large grey disks) is attached to the p(2x2) patch. In each case, the difference in energy (in eV/atom) between a given configuration and the lowest energy configuration is given both for Pd (top line) and Pt (bottom line). Cu(S) atoms are denoted with small circles.

Fig. 11: Energy level spectrum for Pd (top) and Pt (bottom) on Cu(100). For an increasing number of deposited atoms (N), the evolution of the states where the Pd (or Pt) atom is located in the first layer below the surface (1b), noted with a thin line, or in the second layer below the surface (2b), noted with a dashed line. The lowest energy state correspond to a c(2x2) pattern for Pd and a

p(2x2) pattern for Pt. The energy of the (1b) and (2b) levels (in eV/atom) is measured with respect to the lowest energy state.

Fig. 12: Detailed labeling of the configurations shown in Fig. 2.b and 2.c, respectively (see Table 2). Only atoms in the surface plane and first plane below the surface are shown. Surface Cu atoms are denoted with open circles while Cu atoms in the overlayer are denoted with open circles with a darker edge. The adatom (Pd or Pt) is denoted with a black disk.

Fig. 13: Detailed labeling of the configurations shown in Fig. 8.a and 8.b (see Table 3). Only atoms in the surface plane and first plane below the surface are shown. Atom #8 is located two planes below atom #1. Atoms #4 and #3 are replaced by either Pt or Pd to form a p(2x2) or c(2x2) patch, respectively. Surface Cu atoms are denoted with open circles while Cu atoms in the overlayer are denoted with open circles with a darker edge. The adatom (Pd or Pt) is denoted with a black disk.

	Lattice parameter (Å)	Cohesive energy (eV)	Bulk modulus (GPa)	p	$\alpha(Å^{-1})$	$l(Å^{-1})$	$\lambda(Å)$
Cu	3.615	3.50	142.12	6	2.935	0.272	0.765
Pd	3.890	3.94	195.77	8	3.612	0.237	0.666
Pt	3.920	5.85	283.54	10	4.535	0.237	0.666
BFS parameters (in $Å^{-1}$)							
Δ_{CuPt}	-0.0585			Δ_{CuPd}	−0.0431		
Δ_{PtCu}	-0.0441			Δ_{PdCu}	-0.0495		

Table 1

$X(S)Cu(O)_f$

L	m	Atom	X	e^S	g	e^C	e_T
[1]	1	Cu(O)	Pt	2.31049	0.10421	0.0	2.31049
			Pd	2.31049	0.10421	0.0	2.31049
[2]	4	$Cu(S)_1$	Pt	0.64190	0.45922	0.0	0.64190
			Pd	0.64190	0.45922	0.0	0.64190
[3]	1	$Cu(1b)_1$	Pt	0.0	0.99999	0.0	0.0
			Pd	0.0	0.99999	0.0	0.0
[4]	1	X(S)	Pt	0.56100	0.59535	-0.59553	0.20646
			Pd	0.72090	0.45978	-0.37408	0.54891
[5]	4	$Cu(S)_2$	Pt	0.96744	0.35591	-0.03971	0.95331
			Pd	0.96744	0.35591	-0.04487	0.95147
[6]	4	$Cu(S)_3$	Pt	0.96744	0.35591	-0.00019	0.96737
			Pd	0.96744	0.35591	-0.00021	0.96737
[7]	4	$Cu(1b)_2$	Pt	1.410^{-6}	0.99909	-0.00200	-0.00200
			Pd	1.410^{-6}	0.99909	-0.00258	-0.00258
[8]	1	Cu(2b)	Pt	0.0	1.0	-4.10^{-8}	~0
			Pd	0.0	1.0	-6.10^{-8}	~0

Table 2.a

$X(S)Cu(O)_1$

L	m	Atom	X	e^S	g	e^C	e_T
[1]	1	Cu(O)	Pt	2.31049	0.10421	-0.03851	2.30648
			Pd	2.31049	0.10421	-0.04354	2.30596
[2]	1	X(S)	Pt	0.18715	0.75796	-0.53943	-0.22171
			Pd	0.34690	0.61088	-0.37644	0.11594
[3]	2	$Cu(S)_1$	Pt	0.96744	0.35591	-0.03971	0.95331
			Pd	0.96744	0.35591	-0.04487	0.95147
[4]	2	$Cu(S)_2$	Pt	0.64190	0.45922	-0.03738	0.62473
			Pd	0.64190	0.45922	-0.04222	0.62251
[5]	1	$Cu(S)_3$	Pt	0.64190	0.45922	-0.00017	0.64182
			Pd	0.64190	0.45922	-0.00019	0.64181
[6]	3	$Cu(S)_4$	Pt	0.96744	0.35591	-0.00018	0.96737
			Pd	0.96744	0.35591	-0.00021	0.96737
[7]	3	$Cu(1b)_1$	Pt	1.410^{-6}	0.99909	-0.00200	-0.00200
			Pd	1.410^{-6}	0.99909	-0.00021	-0.00258
[8]	1	$Cu(1b)_2$	Pt	0.0	1.0	-0.00258	-0.00211
			Pd	0.0	1.0	-0.00271	-0.00271
[9]	1	Cu(2b)	Pt	0.0	1.0	-4.10^{-8}	~0.0
			Pd	0.0	1.0	6.10^{-8}	~0.0

Table 2.b

Patch	X	Total strain energy	Total chemical energy	Total energy
c(2x2)	Pt	24.64922	-1.77175	22.87747
	Pd	24.92582	-1.425787	23.50003
p(2x2)	Pt	24.19622	-1.92265	22.23124
	Pd	24.83522	-1.29693	23.53828

Table 3

	X/p(2x2)		X/c(2x2)	
Layer	Pt	Pd	Pt	Pd
(O)	6.55580	6.55148	6.52272	6.51408
(S)	15.7078	17.0286	16.4058	17.0520
(1b)	-0.03232	-0.04180	-0.05104	-0.06604

Table 4

X/p(2x2)

L	m	Atom	X	e^S	g	e^C	e_T
[1]	4	Cu(O)	Pt	1.64721	0.20468	-0.04036	1.63895
			Pd	1.64721	0.20468	-0.04563	1.63787
[2]	1	$Cu(S)_1$	Pt	1.410^{-6}	0.99909	-0.00258	-0.00211
			Pd	1.410^{-6}	0.99909	-1.410^{-6}	~0
[3]	4	$Cu(S)_2$	Pt	0.34493	0.59028	-0.06366	0.30735
			Pd	0.34493	0.59028	-0.07169	0.30261
[4]	4	X(S)	Pt	0.18715	0.75796	-0.53942	-0.22171
			Pd	0.34690	0.61088	-0.37644	0.11694
[5]	4	$Cu(S)_3$	Pt	0.96744	0.35591	-0.00037	0.96731
			Pd	0.96744	0.35591	-0.00041	0.96729
[6]	8	$Cu(S)_4$	Pt	0.96744	0.35591	-0.03971	0.95331
			Pd	0.96744	0.35591	-0.04487	0.95147
[7]	4	$Cu(S)_5$	Pt	0.96744	0.35591	-0.00018	0.96737
			Pd	0.96744	0.35591	-0.00021	0.96737
[8]	4	$Cu(1b)_1$	Pt	~0	~1	-0.00211	-0.00211
			Pd	~0	~1	-0.00271	-0.00271
[9]	8	$Cu(1b)_2$	Pt	1.410^{-6}	0.99909	-0.00200	-0.00199
			Pd	1.410^{-6}	0.99909	-0.00258	-0.00258
[10]	4	$Cu(1b)_3$	Pd	1.410^{-6}	0.99909	-0.00200	-0.00199
			Pt	1.410^{-6}	0.99909	-0.00258	-0.00258

Table 5.a

X/c(2x2)

L	m	Atom	X	e^S	g	e^C	e_T
[1]	4	Cu(O)	Pt	1.64721	0.20468	-0.08078	1.63068
			Pd	1.64721	0.20468	-0.09132	1.62852
[2]	1	$Cu(S)_1$	Pt	1.410^{-6}	0.99909	-0.03777	-0.03773
			Pd	1.410^{-6}	0.99909	-0.04950	-0.04945
[3]	4	X(S)	Pt	0.00343	0.96595	-0.36835	-0.35238
			Pd	0.07258	0.81430	-0.31223	-0.18167
[4]	4	$Cu(S)_2$	Pt	0.64190	0.45922	-0.07432	0.60777
			Pd	0.64190	0.45922	-0.08388	0.60338
[5]	4	$Cu(S)_3$	Pt	0.96744	0.35591	-0.03971	0.95331
			Pd	0.96744	0.35591	-0.04487	0.95147
[6]	8	$Cu(S)_4$	Pt	0.96744	0.35591	-0.00018	0.96737
			Pd	0.96744	0.35591	-0.04487	0.95147
[7]	4	$Cu(S)_5$	Pt	0.96744	0.35591	0.0	0.96744
			Pd	0.96744	0.35591	-0.04487	0.95147
[8]	4	$Cu(1b)_1$	Pt	~0	~1	-0.00878	-0.00878
			Pd	~0	~1	-0.01135	-0.01135
[9]	8	$Cu(1b)_2$	Pt	1.410^{-6}	0.99909	-0.00200	-0.00199
			Pd	1.410^{-6}	0.99909	-0.00258	-0.00258
[10]	4	$Cu(1b)_3$	Pd	1.410^{-6}	0.99909	0.0	~0
			Pt	1.410^{-6}	0.99909	0.0	~0

Table 5.b

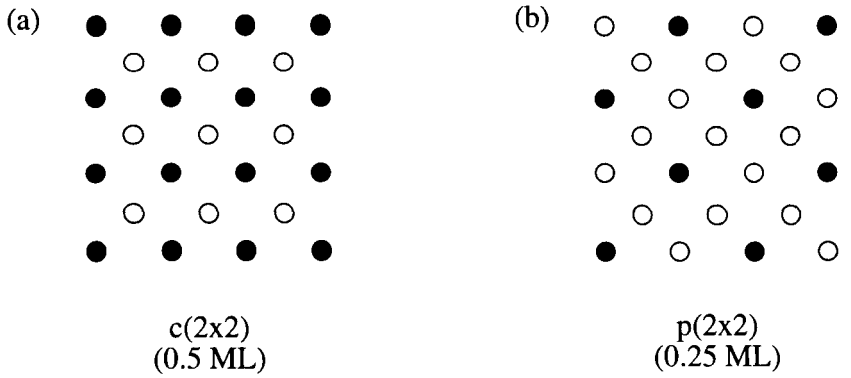

c(2x2)
(0.5 ML)

p(2x2)
(0.25 ML)

Fig. 1

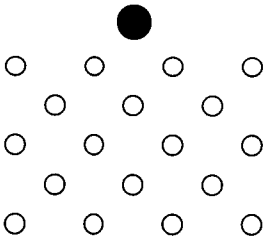

(a) X(O)

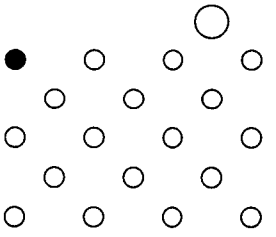

(b) $X(S)Cu(O)_f$

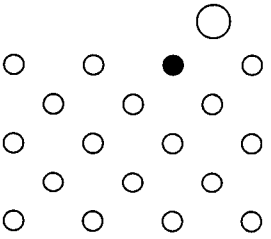

(c) $X(S)Cu(O)_l$

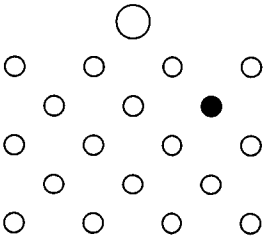

(d) X(1b)Cu(O)

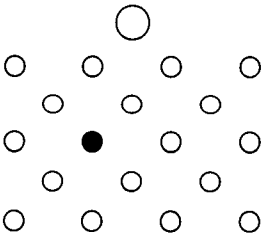

(e) X(2b)Cu(O)

Fig. 2

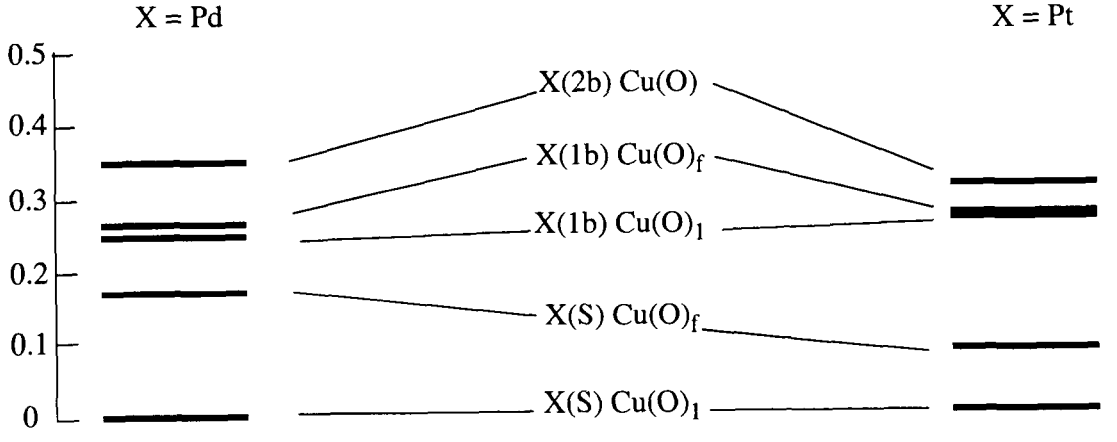

Fig. 3

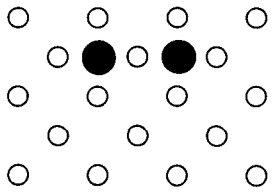

(a) $X(O)X(O)_2$

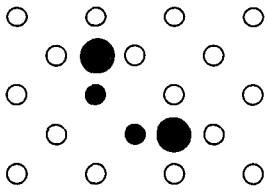

(b) $Cu(O)X(S)_1X(S)_1Cu(O)_1$

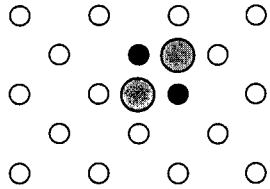

(c) $X(S)X(S)_1Cu(O)_{11}Cu(O)_{111}$

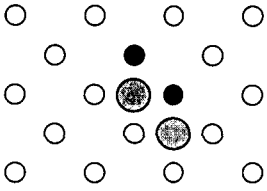

(d) $X(S)X(S)_1Cu(O)_{11}Cu(O)_{11f}$

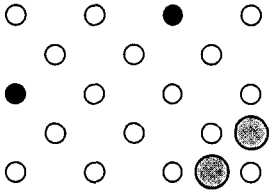

(e) $X(S)+X(S)+Cu(O)Cu(O)_1$

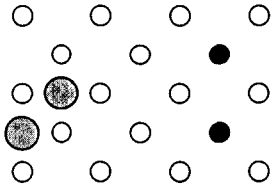

(f) $X(S)X(S)_2+Cu(O)Cu(O)_1$

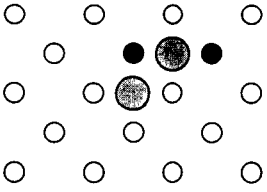

(g) $X(S)X(S)_2Cu(O)_{11}Cu(O)_{11f}$

'c(2x2)'

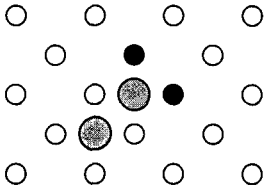

(h) $X(S)X(S)_1Cu(O)_{11}Cu(O)_{1ff}$

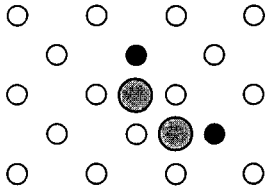

(i) $X(S)Cu(O)_1Cu(O)_1X(S)_1$

'p(2x2)'

Fig. 4

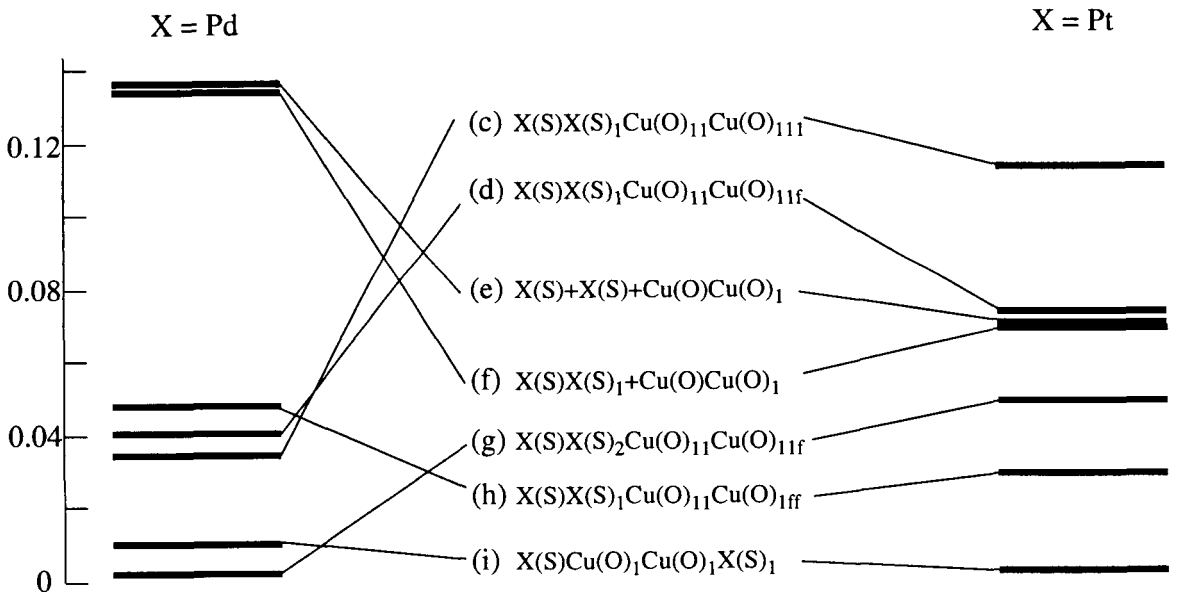
X = Pd
X = Pt
0.12
0.08
0.04
0
(c) X(S)X(S)1Cu(O)11Cu(O)111
(d) X(S)X(S)1Cu(O)11Cu(O)11f
(e) X(S)+X(S)+Cu(O)Cu(O)1
(f) X(S)X(S)1+Cu(O)Cu(O)1
(g) X(S)X(S)2Cu(O)11Cu(O)11f
(h) X(S)X(S)1Cu(O)11Cu(O)1ff
(i) X(S)Cu(O)1Cu(O)1X(S)1

Fig. 5

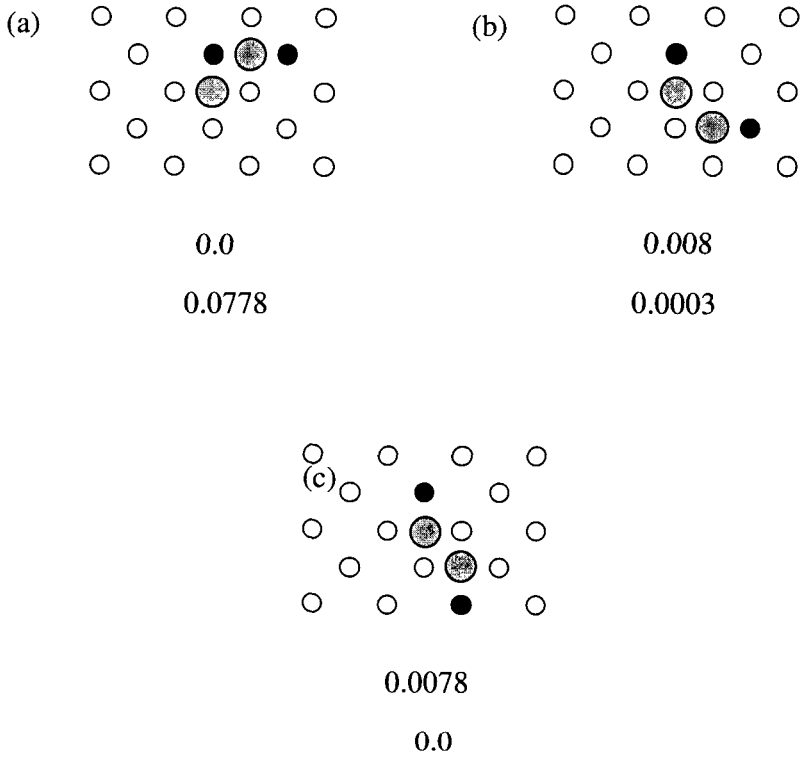

Fig. 6

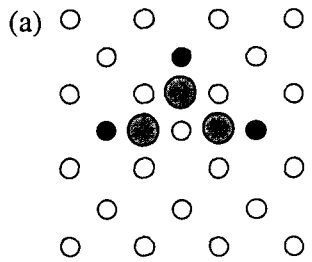

0.0066
0.0

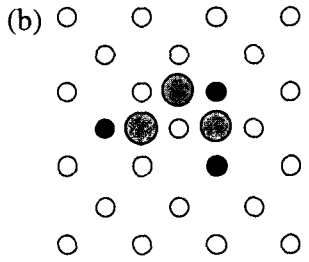

0.0040
0.0542

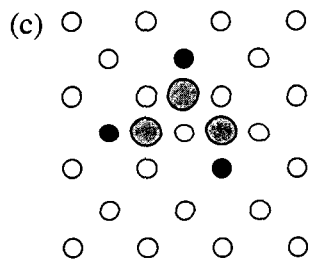

0.0073
0.0007

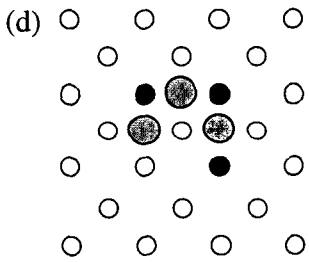

0.0
0.1070

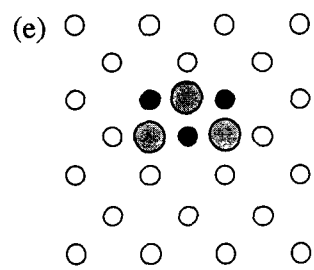

0.3675
0.1244

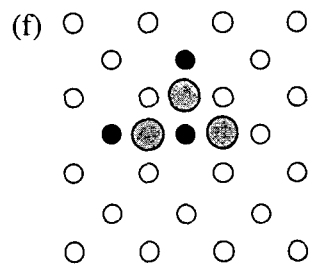

0.1969
0.0900

Fig. 7

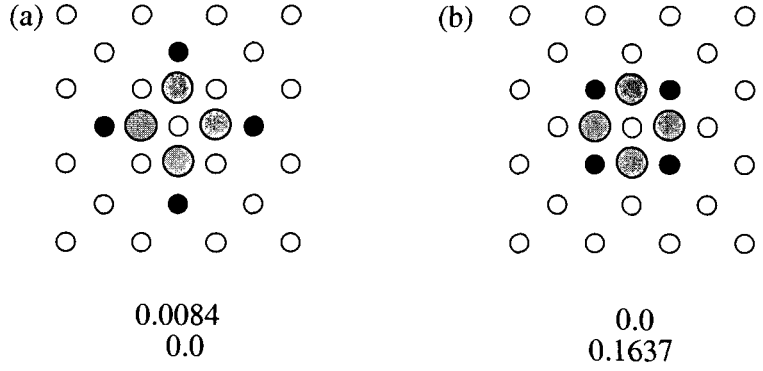

Fig. 8

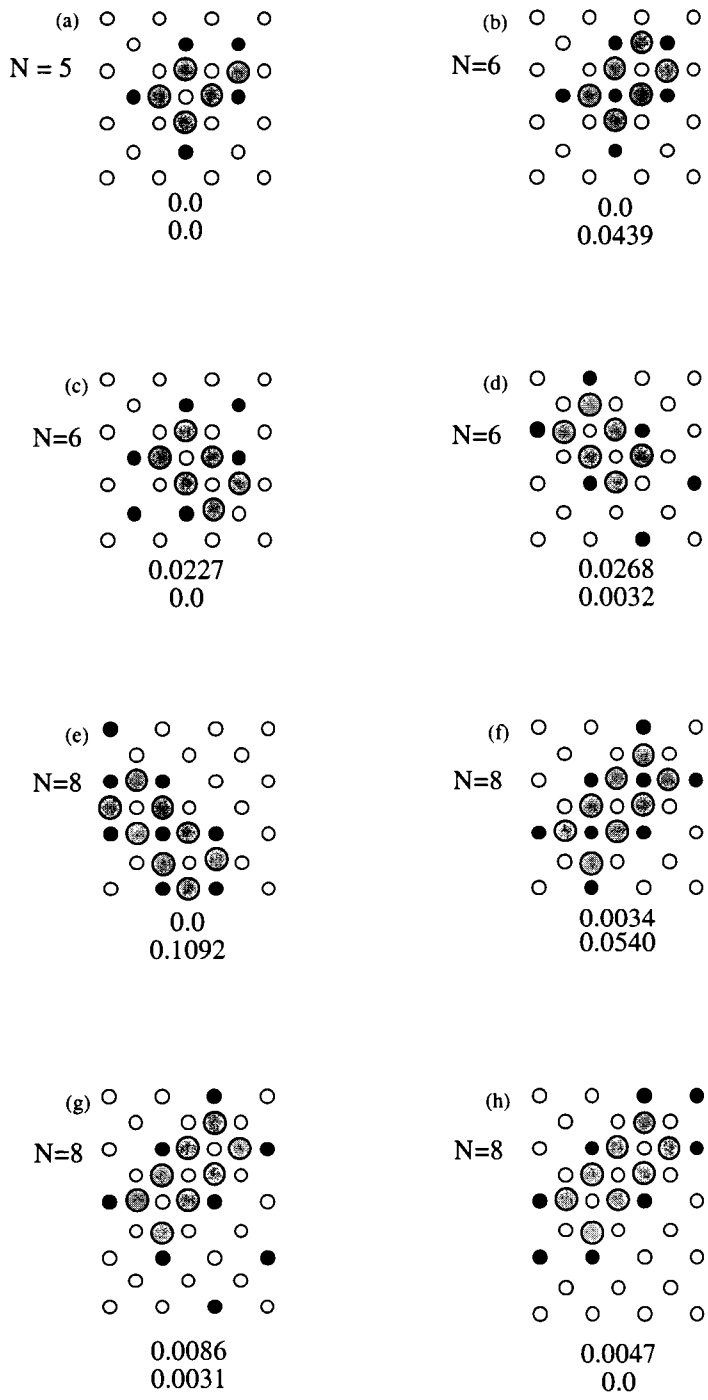
(a)
N = 5
0.0
0.0
(b)
N=6
0.0
0.0439
(c)
N=6
0.0227
0.0
(d)
N=6
0.0268
0.0032
(e)
N=8
0.0
0.1092
(f)
N=8
0.0034
0.0540
(g)
N=8
0.0086
0.0031
(h)
N=8
0.0047
0.0

Fig. 9

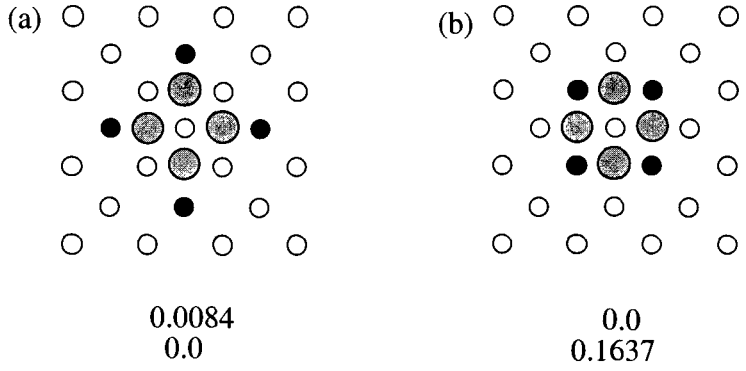

Fig. 10

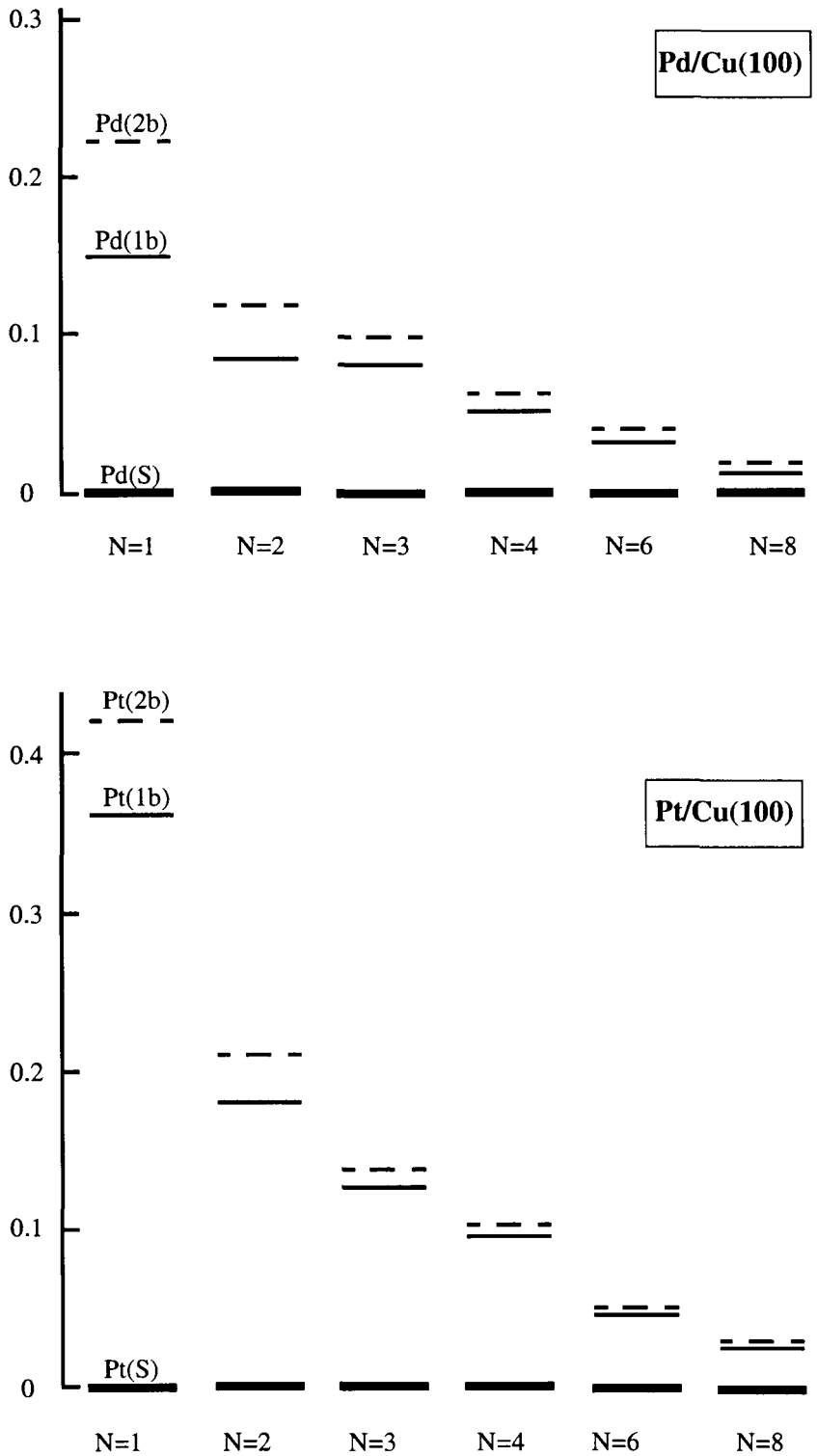
0.3
0.2
0.1
0
Pd(2b)
Pd(1b)
Pd(S)
Pd/Cu(100)
N=1
N=2
N=3
N=4
N=6
N=8
0.4
0.3
0.2
0.1
0
Pt(2b)
Pt(1b)
Pt(S)
Pt/Cu(100)
N=1
N=2
N=3
N=4
N=6
N=8

Fig. 11

(a)

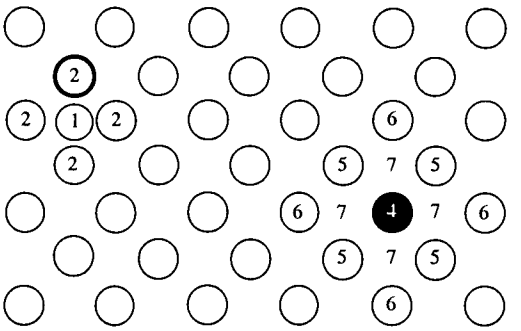

(b)

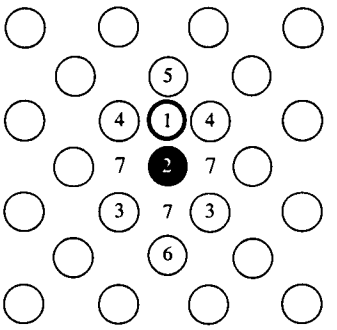

Fig. 12

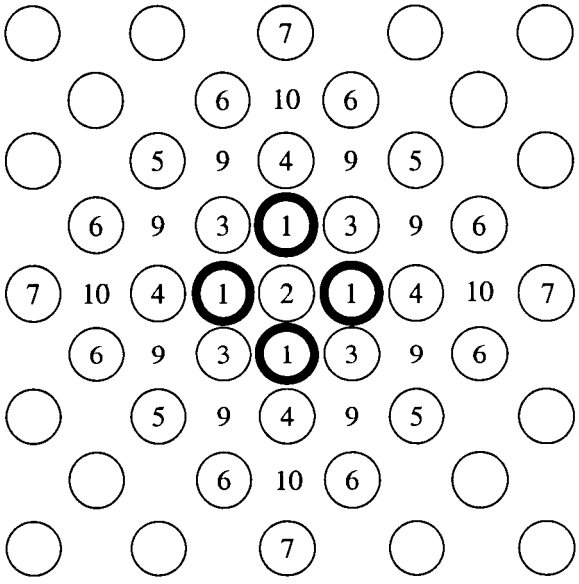

Fig. 13